2023

SPATIALLY RESOLVED ELASTIC MODULUS OF MAGNESIUM SILICATE HYDRATE: A CEMENTITIOUS MATERIAL

Arif Syed

SPATIALLY RESOLVED ELASTIC MODULUS OF MAGNESIUM SILICATE HYDRATE: A CEMENTITIOUS MATERIAL

by

ARIF SYED

THESIS

Submitted in partial fulfillment of the requirements for the degree of Master of Science at The University of Texas at Arlington December, 2023

Arlington, Texas

Supervising committee:

Dr. Efstathios “Stathis” I. Meletis

Dr. Erika La Plante

Dr. Konsta-Gdoutos, Maria

Dr. Ye Cao

ABSTRACT

SPATIALLY RESOLVED ELASTIC MODULUS OF MAGNESIUM SILICATE HYDRATE: A CEMENTITIOUS MATERIAL

ARIF SYED, M.S. (Materials Science and Engineering)

The University of Texas at Arlington, 2023

Supervising professor: Dr. Erika La Plante

Magnesium-based cements such as magnesium silicate hydrate (MSH) have drawn interest as an environmentally friendly substitute for ordinary Portland cement because of their potential for reduced carbon footprint. The precise determination of these materials' elastic moduli is important to better assess their mechanical performance. Atomic force microscopy (AFM) is an effective tool for precise and spatially resolved quantification of nanomechanical characteristics of materials, including thin films. In this study, elastic modulus maps of MSH grown on single crystal mica surfaces were obtained using amplitude modulation-frequency modulation AFM. The effects of the Mg:Si ratio and morphology on the elastic modulus of MSH overgrowths were investigated. Using mica as a reference material, the results reveal elastic moduli ranging from 5 to 15 GPa and 40 to 64 GPa, depending on the growth reaction time and overgrowth morphology. The findings of this study demonstrate the effectiveness of AFM in describing the mechanical characteristics of cementitious phases and suggest that MSH-based materials have a significant potential for use in a variety of construction and building applications.

Keywords: mechanical properties, atomic force microscopy, amplitude modulation-frequency modulation, cement.

ACKNOWLEDGEMENTS

The authors acknowledge financial support provided by the National Science Foundation (NSF CAREER Award #2143159). This work is performed at the Materials Chemistry Laboratory (MCL), the Center for Advanced Construction Materials (CACM), and the Characterization Center for Materials and Biology (CCMB) at the University of Texas at Arlington. The authors acknowledge the support that has made the operations of these laboratories possible. I express my sincere gratitude to my supervising professor for their invaluable guidance and unwavering support throughout the research process. Their expertise, encouragement, and insightful feedback have been instrumental in shaping the direction of this work. I am truly grateful for the mentorship provided, which has greatly contributed to my academic and research growth. I thank Trinh Thao My Nguyen for helping me prepare the samples for characterizations. The contents of this paper reflect the views and opinions of the authors, who are responsible for the accuracy of the datasets presented herein, and do not reflect the views and/or polices of the agency, nor do the contents constitute a specification, standard or regulation.

LIST OF FIGURES

Figures **Page**

LIST OF TABLES

Table **Page**

ABSTRACT

SPATIALLY RESOLVED ELASTIC MODULUS OF MAGNESIUM SILICATE HYDRATE: A CEMENTITIOUS MATERIAL

ARIF SYED, M.S. (Materials Science and Engineering)

The University of Texas at Arlington, 2023

Supervising professor: Dr. Erika La Plante

Magnesium-based cements such as magnesium silicate hydrate (MSH) have drawn interest as an environmentally friendly substitute for ordinary Portland cement because of their potential for reduced carbon footprint. The precise determination of these materials' elastic moduli is important to better assess their mechanical performance. Atomic force microscopy (AFM) is an effective tool for precise and spatially resolved quantification of nanomechanical characteristics of materials, including thin films. In this study, elastic modulus maps of MSH grown on single crystal mica surfaces were obtained using amplitude modulation-frequency modulation AFM. The effects of the Mg:Si ratio and morphology on the elastic modulus of MSH overgrowths were investigated. Using mica as a reference material, the results reveal elastic moduli ranging from 5 to 15 GPa and 40 to 64 GPa, depending on the growth reaction time and overgrowth morphology. The findings of this study demonstrate the effectiveness of AFM in describing the mechanical characteristics of cementitious phases and suggest that MSH-based materials have a significant potential for use in a variety of construction and building applications.

Keywords: mechanical properties, atomic force microscopy, amplitude modulation-frequency modulation, cement.

TABLE OF CONTENTS

CHAPTER ONE

1. INTRODUCTION

Magnesium silicate hydrate (MSH) is a potential alternative to conventional Portland cement.[1–4] This is particularly crucial considering the depletion of calcium, a natural resource that is heavily mined and necessary to create Portland cement to meet the demands of both small-scale and large-scale construction projects.[5–8] By employing MSH as an alternative to cement, we can reduce the strain on calcium resources while also taking advantage of the plentiful magnesium supply. However, the use of MSH in construction applications is currently limited, due to a lack of knowledge regarding its cementitious qualities, particularly its mechanical properties, durability, and long-term performance.

The elastic modulus of cementitious materials describes their capacity to endure elastic deformation under applied stresses. The composition, water-to-cement ratio, curing conditions, and aggregate qualities all affect the elastic modulus of cementitious materials.[9,10] It is a crucial criterion for evaluating the strength, resilience, and overall performance of cement-based systems. For instance, in applications where stiffness and load-bearing capability are crucial, such as high-rise buildings or bridge constructions, a greater elastic modulus implies a more rigid material that can efficiently resist deformation and convey stress.[11] On the contrary, a lower elastic modulus is characteristic of a more flexible material that can withstand loads and motions, which is preferable for applications requiring compatibility with thermal expansion or fracture resistance, such as pavements or constructions exposed to large temperature fluctuations.[12,13] Therefore, designing and assessing structures, improving material formulations, and assuring the durability and serviceability of concrete structures all depend on an understanding and characterization of the elastic modulus.

Previous studies and research on elastic modulus of cementitious materials has been a significant focus in materials science and civil engineering. Various experimental techniques and findings have been explored to understand the behavior of these materials. Some common techniques and findings from previous literature are Static and Dynamic Testing, non-destructive testing, nano-indentation, finite element analysis (FEA), molecular dynamic (MD) simulation,

effect of supplementary cementitious materials (SCMs) such as fly ash, silica fume, and slag, high-temperature studies, influence of curing conditions and age, and lastly multiscale approaches.[10] One of the important criteria for cementitious materials is investigating the behavior of these materials under extreme conditions, such as high temperatures, high pressures, or severe loading conditions, to ensure their reliability in diverse construction applications. These extreme conditions can be achieved by improving the elastic modulus of cementitious materials such that it can withstand severe loading conditions. Also, MSH (magnesium silicate hydrate) cements are unexplored pertaining to its precipitation rate, strengthening structural mechanisms, environmental stability, and especially its mechanical properties (elastic modulus).

Therefore, this study mainly focuses on finding the mechanical property (elastic modulus) of magnesium-based cements and proving that the atomic force microscopy (AFM) is a potential tool to characterize the mechanical properties of materials. Investigating MSH's mechanical properties at elevated spatial and temporal resolutions offers the opportunity to comprehend the fundamental origins underlying the characteristics of MSH. Moreover, insights gained from this investigation can be extrapolated to lesser-explored magnesium-based cement. This, in turn, establishes its feasibility as a binding material in construction, serving as a potential alternative to conventional Portland cements.

In this study, we characterize the elastic modulus of MSH grown on single crystal mica using amplitude modulation-frequency modulation atomic force microscopy (AM-FM AFM). To ascertain the distribution of associated phases that form, MSH was also synthesized as bulk powders and characterized using a suite of tools including X-ray diffraction (XRD), thermogravimetric analysis (TGA), Fourier-transform infrared spectroscopy (FTIR), and scanning electron microscopy with energy-dispersive spectroscopy (SEM-EDS). We compare brucite with MSH. This study demonstrates the unique capability of AFM in quantifying mechanical properties of diverse materials such as alternative cements at the nanoscale. The elastic modulus of MSH, measured for the first time in this study, is compared with CSH, and implications on its potential as an alternative construction material are discussed.

CHAPTER TWO

2. EXPERIMENTAL METHODS AND MATERIALS

2.1. *Preparation of samples*

The samples were made by mixing stock solutions of magnesium nitrate hexahydrate ($Mg(NO_3)_2.6H_2O$, 95% purity), sodium metasilicate pentahydrate ($Na_2SiO_3.5H_2O$, 99% purity), and ultrapure water (> 18.2 MΩ·cm) in a polypropylene centrifuge tube, following a previously published procedure.[4] Powder samples were prepared by introducing 6 ml volumes of each stock solution, featuring a final concentration of 100 mM for both Mg and Si into a polypropylene centrifuge tube, resulting in a final volume of 12 ml. The sealed tubes were thoroughly mixed and allowed to react at ambient temperature (25 ± 2 °C) for 48 hours. Following this period, observable precipitates formed and settled at the bottom of the tube. To stop further reaction, 1 ml of ethanol was introduced into the tube. Subsequently, the tube underwent centrifugation at 2500 RPM for 20 minutes in a centrifuging machine to separate the precipitates from excess solution. This process was iterated twice to ensure complete removal of excess solution, leaving only the precipitates. The wet precipitates were then transferred to a larger open container and subjected to drying in a vacuum oven. Upon achieving dryness, the precipitates were finely ground into powder. A similar procedure was followed to prepare the powder sample for brucite using stock solutions of NaOH and $Mg(NO_3)_2$, to directly compare the characterization results of brucite with MSH. The resulting powder sample underwent comprehensive characterization using X-ray diffraction (XRD), Fourier transform infrared spectroscopy (FTIR), thermogravimetric analysis (TGA), and scanning electron microscopy-energy dispersive X-ray spectroscopy (SEM-EDS). Growth solutions, feature a final concentration of 100 mM for both magnesium (Mg) and silicon (Si) with Mg/Si ratio of 1 were employed in the synthesis of MSH samples. Each stock solution, constituting 1 ml with total volume of 2 ml was utilized for preparing the sample for AFM analysis. Along with the sample having Mg/Si ratio 1, we also prepared other 3 different samples with Mg/Si ratios 0.5, 1.5, and 2 to compare and comprehend the variations in the elastic modulus values of MSH for different Mg/Si ratios. A multiparameter benchtop meter (ThermoFisher Scientific Orion™ VersaStar Pro™) calibrated

for pH ranges of 4 to 12, was used to measure the pH values of the growth solution immediately following the mixing of the stock solutions, ranging from 9.486 to 10.590 for different samples (**Table 2**). The reference material and substrate were a single crystal disc of muscovite mica (001), grade V1, Ted Pella, with dimensions of 10 mm in diameter and 0.21 mm in thickness. The mica disc was cleaved to ensure a clean surface, and any debris was successfully removed by a brief exposure to ultra-high purity (UHP) nitrogen gas. The cleaved mica disc is then placed immediately in a centrifuge tube containing 2 ml of growth solution. To allow MSH to precipitate on the mica surface, the tube was sealed and then stored at ambient temperature (25 ± 2 °C) for 48 hours. After 48 hours, the pH values of the growth solutions were once again measured using the previously calibrated multiparameter benchtop meter, ranging from 8.748 to 9.877 for different samples (**Table 2**). These final pH measurements provided valuable information on the extent of MSH precipitation. Following the pH measurements, the mica disc was carefully removed from the centrifuge tube. Excess liquid was removed from the mica disc's edge using a Kimwipe™, and the disc was then briefly exposed to ultra-high purity (UHP) nitrogen gas to ensure the removal of any remaining liquid. Following a similar procedure another sample was prepared with a reaction time of 40 minutes to directly compare the morphological characteristics and elastic modulus values with the sample having 48 hours of reaction time. The samples were then stored in a lidded polyethylene container under ambient conditions until they were ready to be characterized using AFM.

Mica was used as a reference substrate; a reference substrate must have a known elastic modulus value to get the unknown material's (MSH) elastic modulus value quantitatively. To find the elastic modulus value of mica, we used nano-indentation technique. Nano-indentation technique uses a diamond tip that indented on the mica surface at five different areas and the average elastic modulus value was found to be 64 ± 2 GPa. This known elastic modulus of mica is used as reference to find the elastic modulus value of unknown material, in this study the unknown material is MSH.

2.2. *Characterization of MSH powder*

To characterize the molecular structure of the powder precipitates, Bruker D8 Advance X-ray diffractometer was used having CuK_{α} radiation as 1.5418 Å. The data was collected at 2θ from 5° to 80° with an increment of 0.01°, 0.5 degree/min scan rate, and locked couple scan type at a voltage and current of 40 kV and 40 mA respectively.

A Nicolet iS50 FTIR spectrometer made by Thermo Scientific was used to perform infrared absorbance measurements. An attenuated total reflectance (ATR) attachment and a deuterated triglycine sulfate (DTGS) KBr detector were fitted to the apparatus. With the atmospheric suppression option enabled and a wavenumber range of 525 to 4000 cm^{-1}, the infrared spectra were obtained with the following parameters: 32 scans for background and sample.

TGA (Thermogravimetric Analysis) was done using "TA instrument's SDT-Q600 Simultaneous TGA/DSC", The Q600 features a highly reliable horizontal dual-balance mechanism that supports precise TGA and DSC measurements and it also features a rugged, reliable, horizontal furnace encased in a perforated stainless-steel enclosure with a horizontal purge gas system with digital mass flow control and integral gas switching capability. The experiment is performed from the temperature range of 20 °C to 1050 °C with an increment of 15 °C/min and N_2 gas flow at the rate of 20 ml/min. A ceramic cup was used to hold the powder sample on which the experiment is performed. The output graph/signal contains both TGA and DSC data simultaneously.

SEM-EDS (Scanning Electron Microscope - Energy Dispersive X-ray Spectroscopy) was done using "Hitachi S-3000N Variable Pressure SEM", The Hitachi S-3000N is a Variable Pressure SEM with a tungsten electron source. It is capable of imaging specimens at high vacuum and in a variable pressure range from 1-270 Pa. This allows nonconducting specimens to be imaged without coating with a conductive film. The experiment was performed by setting the parameters as an accelerating voltage of 20 kV, magnification of 200X, beam current of 62 nA, and working distance of 15 mm. Using the point and shoot feature of EDS we got the data for selected points on the SEM image that gives the atom % for all the elements present in the sample.

2.3. *Measurement of elastic modulus at the nanoscale*

A nanomechanical tapping method called amplitude modulation-frequency modulation (AM-FM) AFM is used to characterize the elastic modulus of MSH overgrowth. In AM-FM, the amplitude modulation (AM) enables the collection of surface topography while frequency modulation (FM) gives nanomechanical characteristics of the sample surface, particularly the elastic modulus or stiffness. The cantilever's first resonance frequency (A1) is driven with a large amplitude, while the second resonance frequency (A2) is driven with a lesser amplitude simultaneously. The resulting cantilever drive signal (shown in blue) is used in AM-FM viscoelastic mapping mode. After the tip interacts with the sample, this signal is compared to the cantilever detection signal (shown in green). In parallel with the conventional tapping mode, the topography feedback loop employs A1 to monitor surface topography and the sample's viscous response, quantified through loss tangent measurements. Additionally, a secondary feedback loop maintains the constancy of the higher-frequency A2 oscillation. The phase feedback loop is responsible for tracking alterations in the second resonance frequency mode. The observed frequency shifts are subsequently correlated with the elastic properties of the sample through meticulous modeling and referencing to known samples.[14] This mode requires a reference material (herein, single crystal mica having elastic modulus value as 64 ± 2 GPa) with a known elastic modulus value to determine the unknown elastic modulus value of a material (herein, MSH). The known elastic modulus of the reference material is used to obtain the best-fit parameters that describe tip-sample interactions including tip-sample Hertzian contact mode (Hertz Punch, Hertz Cone, Hertz Sphere) and tip geometry (e.g., tip radius and half-cone angle), enabling quantitative determination of the unknown elastic modulus of MSH. AFM data were collected using a silicon probe having a rectangular cantilever with a 70 nm-thick gold coating on the detector side and force constant of 3 N/m, nominal resonance frequency of 75 kHz, length of 225 µm, width of 28 µm, and thickness of 3 µm.

CHAPTER THREE

3. RESULTS AND DISCUSSION

3.1. Analysis of phases present on the sample surface

It is known that the chemical composition of MSH is influenced by several variables, including the reaction durations, chemical composition of precursors, temperature, Mg/Si ratios, and water activity.[15–17] Previous studies characterizing MSH show variations in chemical composition of MSH and the presence and abundance of associated phases such as brucite ($Mg(OH)_2$) and MSH (magnesium silicate hydrate).[18,19] To ascertain that MSH is the predominant phase that forms in the samples characterized by AM-FM, we characterize MSH homogeneously grown in parallel.

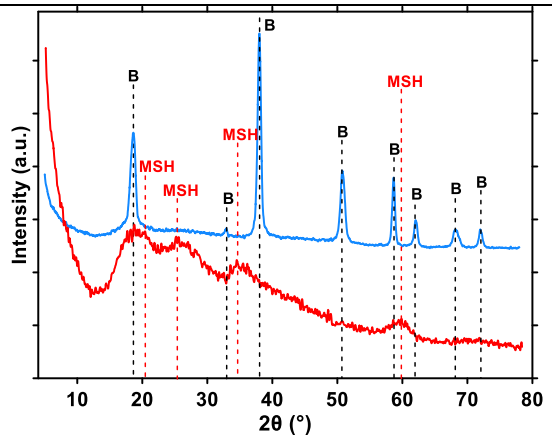

Figure 1. X-ray diffraction pattern of the synthesis of MSH powder sample reacted for 48 hours with Mg/Si ratio 1 at 25 ± 2 °C, showing MSH (red) and Brucite (blue) where B is for brucite, MSH is for magnesium silicate hydrate.

XRD, TGA, and FTIR show that the precipitates are primarily MSH, with small amounts of brucite. Specifically, XRD data for MSH reveal characteristic broad humps at 2θ = 20.1, 26.7, 35.0, and 59.9°.[18–23] To facilitate a direct comparison between the MSH sample (red, **Fig. 1**) and brucite, we prepared a brucite sample (blue, **Fig. 1**) using stock solutions of NaOH and $Mg(NO_3)_2$, subjecting the reaction to a 48-hour duration at a controlled temperature of 25 ± 2 °C with a 1:1 ratio of reactants. The X-ray diffraction (XRD) pattern for the brucite sample closely

aligns with previous research findings,[19] confirming its characteristic crystalline structure (**Fig. 1**). It is evident that brucite is not present in substantial quantities in the MSH sample.

Thermogravimetric analysis (TGA) of MSH reveals weight losses at three distinct regions (**Fig. 2**). The first region (20-250°C) was associated with poorly bound water, including monolayer, multilayer, and interlayer water within MSH.[23–25] This region may also include bulk water at high relative humidity. The second and third regions of water loss, observed above 250 °C, have been attributed to silanol (Si–OH) and magnesium hydroxyl (Mg–OH) groups in MSH.[18]

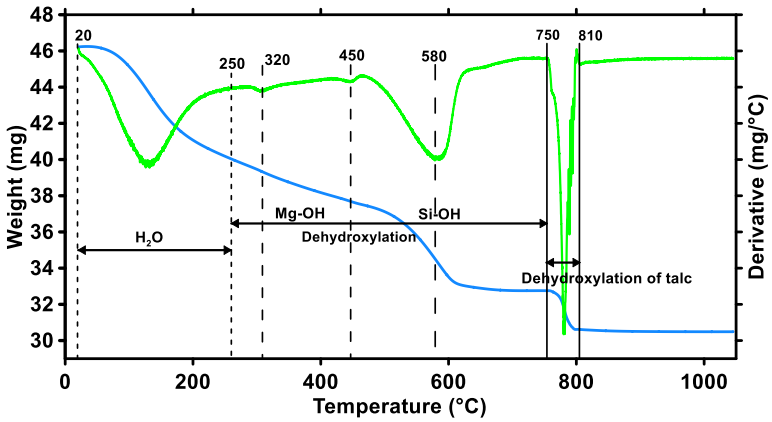

(a)

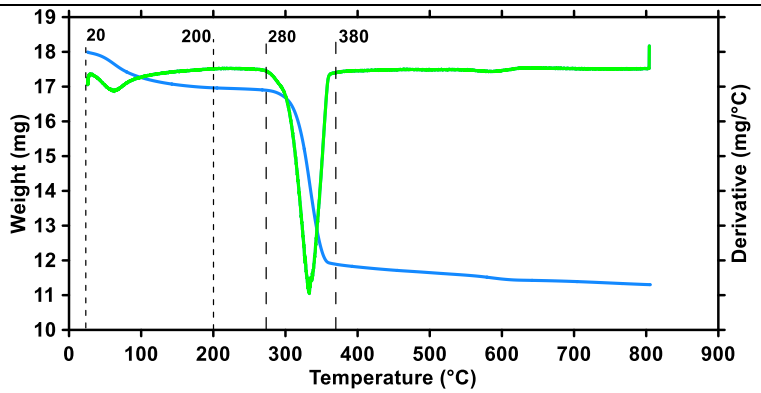

(b)

Figure 2. TGA/dTGA trends of the powder samples reacted for 48 hours at 25 ± 2 °C with a ratio of 1:1, showing **(a)** MSH, **(b)** Brucite.

The second water loss, in the case of MSH with a Mg/Si ratio of 1, is centered at 320 °C and 450 °C and is primarily related to the dehydroxylation of magnesium hydroxyl (Mg-OH) groups.[18,24–27] The third weight loss, occurring at 580 °C, is associated with the dehydroxylation of silanol (Si-OH) groups. The dehydroxylation of the minerals of the serpentine group (hydroxyl groups linked to the magnesium: inner OH and surface OH) has been observed by TGA at 670–900 °C, while the inner OH groups linked to the magnesium in the talc structure dehydroxylates at 750–1000 °C**,** in agreement with the weight loss observed for MSH from 450 to 1000 °C.[28] In contrast, the brucite sample shows a sharp peak at around 320 °C primarily attributed to the release of hydroxyl groups (Mg-OH) (**Fig. 2b**).[27] This peak is present in MSH, albeit very small.

FTIR analysis shows a sharp band at 3692 cm^{-1} confirms the presence of very small amounts of brucite in the MSH samples (red, **Fig.3**) with Mg/Si ratio of 1, as we can clearly confirm that by comparing it with the brucite sample (blue, **Fig. 3**).[19,23,29]

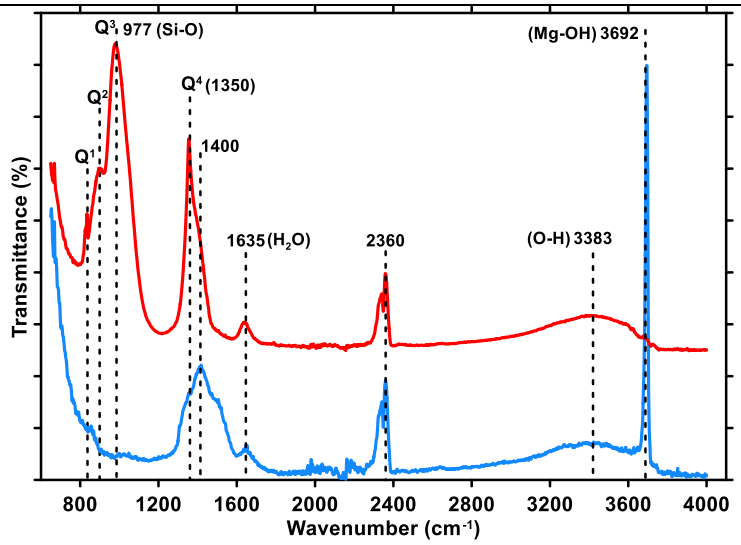

Figure 3. FTIR (Fourier-Transform Infrared) Spectroscopy of the MSH powder samples reacted for 48 hours at 25 ± 2 °C with a Mg/Si ratio of 1, where red curve is for MSH, and blue is for brucite.

The silica tetrahedra polymerization of in MSH (~600-1400 cm^{-1}) can be characterized from the relative amounts of Q^0 (no oxygen sharing between silicon atoms), Q^1 (one oxygen shared

between two silicon atoms), Q^2 (two shared oxygens, forming chains), and Q^3 (three shared oxygens, forming sheets),[30–32] where Q^3 species as representing silica sheets and Q^2 as representing defects within these sheets. Additionally, bands at Q^1 (835cm^{-1}), Q^2 (902 cm^{-1}), Q^3 (977 cm^{-1}), and Q^4 (1350 cm^{-1}) are for MSH samples (**Fig. 3**).[18,19,23,33,34] Well-defined FTIR peaks that correspond to Si–O stretch and O–H stretch and bend, and the increased Q^3/Q^2 sites together with a reduced in Q^1 sites, indicative of increased silica polymerization. These spectral features indicate the persistence of unreacted silica in the lower Mg/Si ratio samples (typically Mg/Si ratios ≤ 1). In the IR spectra, distinct bands related to MSH are observed between ~600 and1400 cm^{-1} and are associated with asymmetric and symmetric Si–O stretching vibrations and a band at around 1635 cm^{-1}, attributed to H–O–H bending vibrations of molecular-bound H_2O (**Fig. 2**).[4,23,35,36] The FT-IR spectra also reveal that the band at 3383 cm^{-1} is associated with OH stretching vibrations of MSH.[4] These bands may also be indicative of a sepiolite-like structure or, at higher Mg/Si ratios, serpentine-like antigorite. Additionally, the FT-IR data suggests that MSH phases contain hydroxyl groups bound to silicon and magnesium, as well as physically bound and adsorbed water.[18]

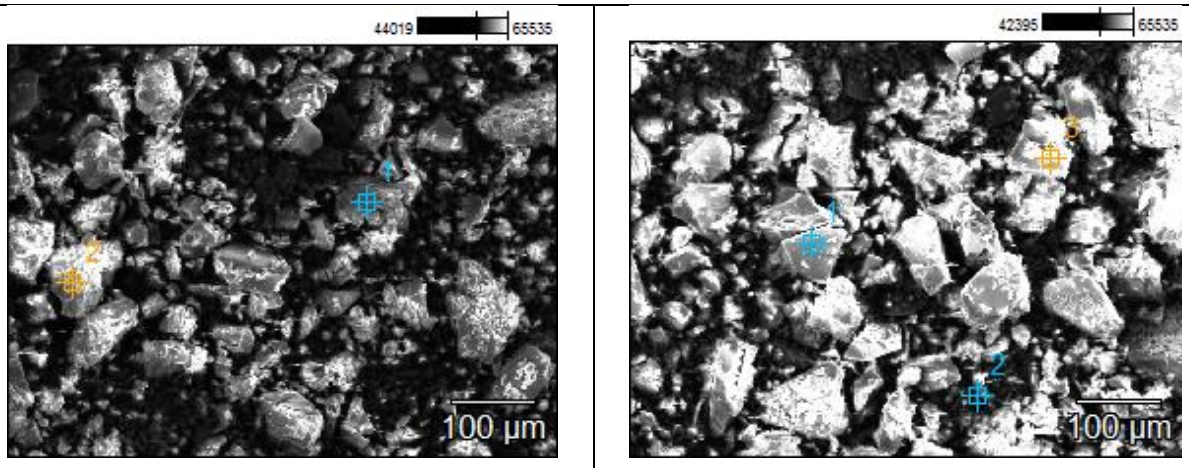

(a) **(b)**

Figure 4. SEM-EDS (Scanning Electron Microscopy) of the MSH powder samples reacted for 48 hours at 25 ± 2 °C with Mg/Si ratio of 1, showing **(a)** Image for points 1 and 2 in table 1 and for AREA 1 in table 2, **(b)** Image for points 3,4, and 5 in table 1 and for AREA 2 in table 2.

The SEM-EDS analysis (**Fig. 4**) revealed Mg to Si ratios for MSH are ranging from 0.64 to 1.02, with an average of 0.852, suggesting a relatively uniform distribution of Mg and Si within the precipitate and the predominance of MSH (**Table 1**). It is important to highlight that the atom % values for Mg/Si remain close to 1, aligning with the initial Mg/Si ratio of 1.[22,34] Taken together, the combination of analytical techniques shown herein provides compelling evidence for the persistence of primarily MSH in the samples, with minor amounts of brucite.

Table 1. SEM-EDS analysis of MSH sample, showing the **atom %** data for each selected individual points on the images using point and shoot feature of EDS having total of 5 points along with the **atom %** data for whole image area using spectral imaging feature of EDS having total of 2 areas.

Points	**Elements**					**Mg/Si**
	N	**O**	**Na**	**Mg**	**Si**	
1	1.63	67.26	5.19	13.10	12.82	1.02
2	1.35	67.29	3.42	13.82	14.12	0.98
3	0.00	54.06	2.93	16.68	26.32	0.64
4	0.00	63.32	4.44	14.59	17.65	0.83
5	3.23	59.76	7.13	13.17	16.71	0.79
					AVG =>	**0.852**
Area						
1	0.00	63.97	7.23	13.40	15.39	0.87
2	0	63	8	12	14	0.86
					AVG =>	**0.865**

3.2. *Influence of morphology and reaction time on the elastic modulus of MSH*

The AMFM analysis is a method that must be done quantitatively, meaning that the sample must have a known substrate/reference material (mica) with a known elastic modulus value (64 ± 2) to find the mechanical properties (elastic modulus) of the unknown material (MSH). The

bright area in **Fig. 5c,** that does not contain any precipitates is mica and the rest are the MSH precipitates that are formed after supersaturated solutions of MSH reacts with mica surface for reaction duration of 48 hours. The development of precipitates on the mica surface is not uniform and formed in two different morphologies. One that is faceted/big more or like crystalline and other is irregular/small more or like amorphous. If we look at **Fig. 5d,** this graph shows the elastic modulus data for the entire area of the elastic modulus map (**Fig. 5c**).

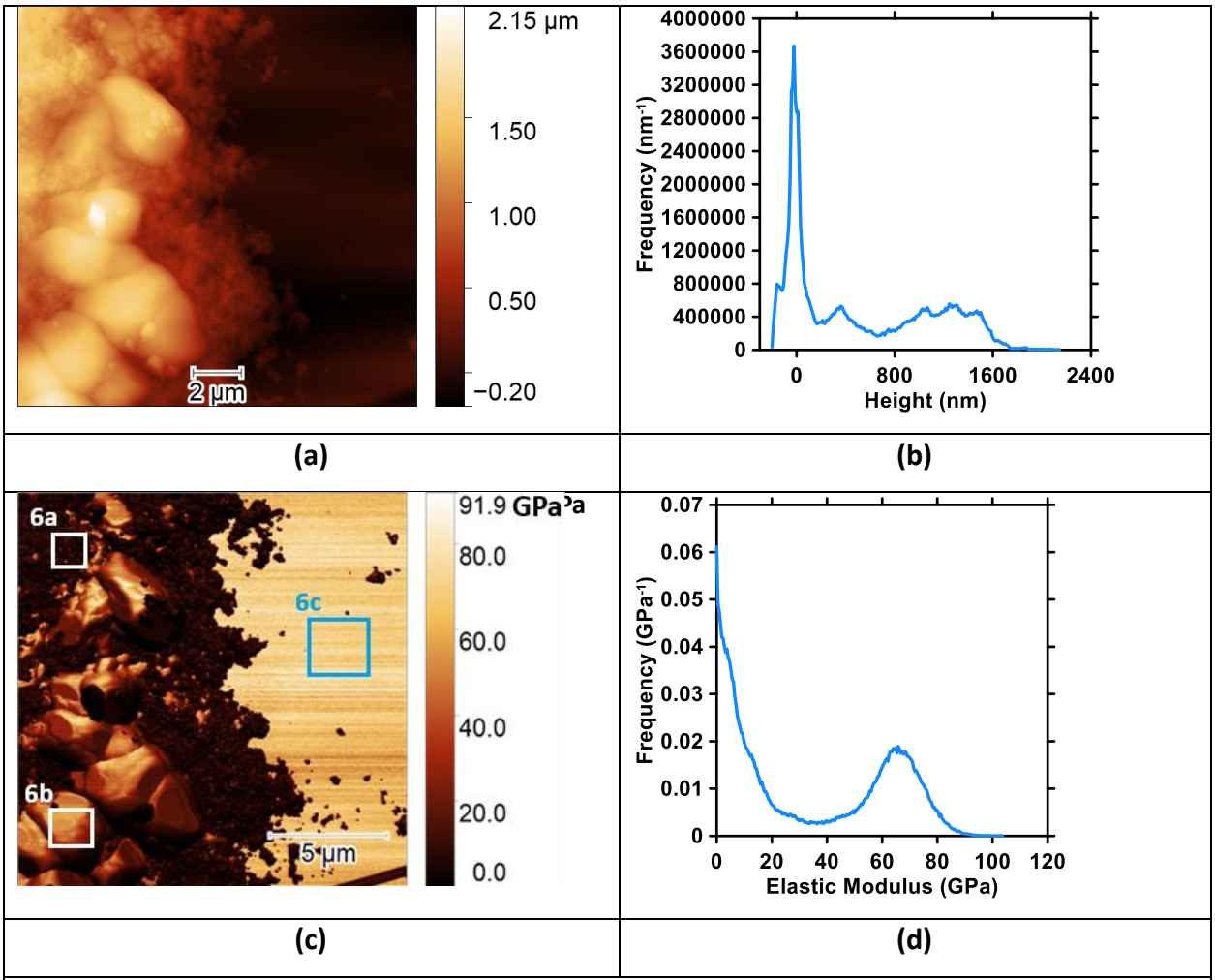

Figure 5. Atomic force microscopy images of precipitates grown on mica substrate after reacting with supersaturated solution of MSH for 48 hours at 25 °C with final concentration of Mg = 100 mM; Si = 100 mM; Mg/Si = 1, taken using amplitude modulation & frequency modulation mode, showing **(a)** height map, **(b)** height distribution graph, **(c)** elastic modulus map, and **(d)** elastic modulus graph.

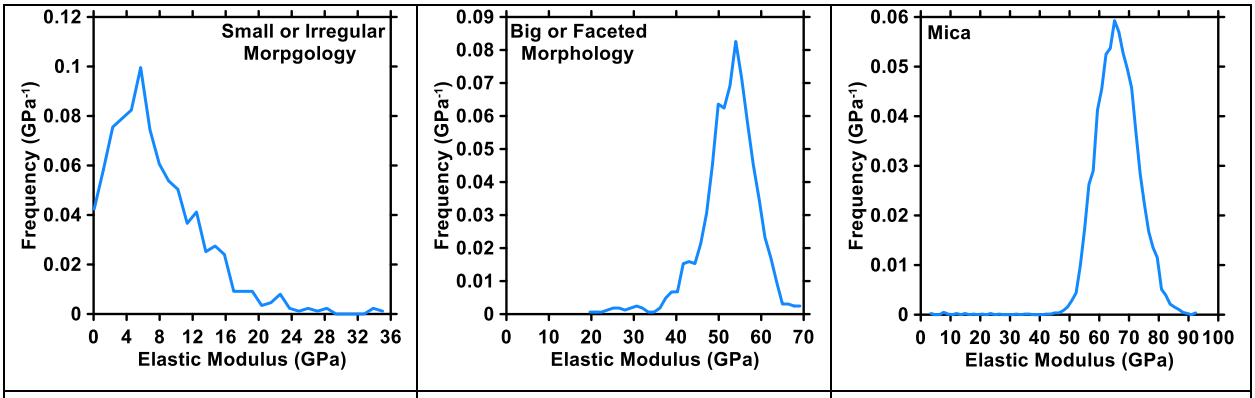

Figure 6. Highlighted cropped-in atomic force microscopy images of precipitates grown on mica substrate after reacting with supersaturated solution of MSH for 48 hours at 25 °C with final concentration of Mg = 100 mM; Si = 100 mM; Mg/Si = 1, taken using amplitude modulation & frequency modulation mode, showing **(a)** cropped-in graph for irregular morphology MSH at 6 GPa, **(b)** cropped-in graph for faceted morphology MSH at 54 GPa, and **(c)** cropped-in graph for mica substrate set at 65 GPa for the elastic modulus map shown in **Fig. 5c**.

In this study, we conducted a detailed analysis of elastic modulus values within distinct areas of interest on a sample surface containing MSH (magnesium silicate hydrate) precipitates (**Fig. 6**). The results revealed significant variations in elastic modulus, with irregular or small morphological characteristics of MSH precipitates exhibiting a lower modulus of 6 GPa (**Fig. 6a, 7d, and 7e**), indicating greater compliance. In contrast, MSH precipitates with faceted or big morphological features displayed a higher elastic modulus of 54 GPa (**Fig. 6b**), and for other areas on the sample it displayed a modulus of 64 GPa (**Fig. 7b, 7c**) and in some areas as close to 75 GPa, signifying increased stiffness and resistance to deformation. This study also established a clear correlation between the morphological characteristics and the mechanical properties, specifically the elastic modulus of MSH. Different regions of the sample surface, characterized by varying morphological features, demonstrated discrete elastic modulus values, highlighting the role of morphological control in fine-tuning the elastic modulus of MSH-based cements. Wherever we have irregular or small morphological characteristics, we get lower elastic

modulus whereas higher elastic modulus values for faceted or big morphological characteristics. This insight suggests potential applications in construction where customized elastic modulus can enhance structural integrity and overall performance.

Table 2. Experimental conditions for all MSH samples, showing Mg/Si ratios, final concentration of Mg and Si, initial pH measured immediately after mixing, final pH measured after certain duration of reaction, time of reaction, and reaction temperature.

Mg/Si	Mg (mM) (Final Conc.)	Si (mM) (Final Conc.)	pH (initial)	pH (final)	Time (h)	Temp. (°C)
0.5	50	100	10.187	9.852	48.281	23.1
1	100	100	10.286	9.877	0.67	22.3
1	100	100	10.158	9.766	0.67	23.1
1	100	100	10.395	9.623	24.636	22.9
1	100	100	10.395	9.575	24.564	22.9
1	100	100	10.287	9.461	94.131	22.3
1	100	100	10.414	9.455	112.489	23.1
1	100	100	10.590	9.621	48.05	24.1
1.5	150	100	9.560	9.096	0.67	23.1
1.5	150	100	9.724	9.462	48.075	23.3
2	200	100	9.486	9.035	0.67	24
2	200	100	9.729	8.748	48.10	23.3

For comparison, the elastic modulus of brucite was found to be 11 GPa in a previous study using Neutron diffraction data suitable for Rietveld refinements that were collected on a powder sample of synthetic Mg $(OH)_2$ by the Polaris time-of-flight spectrometer.[37] In another study the second-order elastic constants of brucite were determined by Brillouin scattering to 15 GPa in a diamond anvil cell.[38] Similarly, from previous studies the elastic modulus of silica was investigated through various techniques. The ASR gel's density was determined as a function of pressure using X-ray absorption, yielding an isothermal bulk modulus of 33 ± 2 GPa. Brillouin spectroscopy measured isentropic bulk (24.9–34.0 GPa) and shear moduli (8.7–10.1 GPa) of the gel.[39] In a separate study, amorphous SiO_2 nanowires with diameters of 50 to 100 nm were

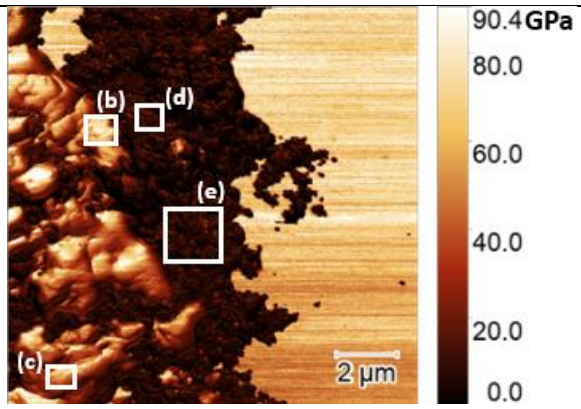

(a)

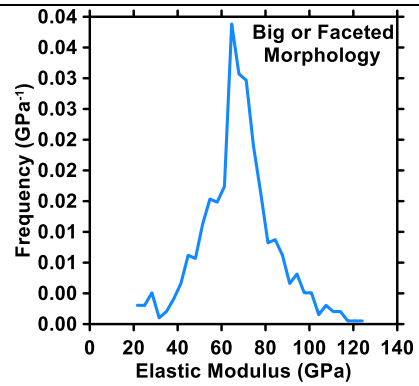

(b)

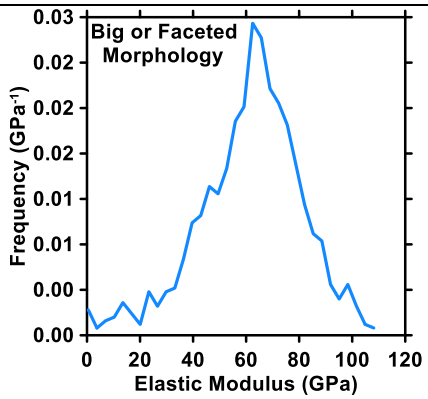

(c)

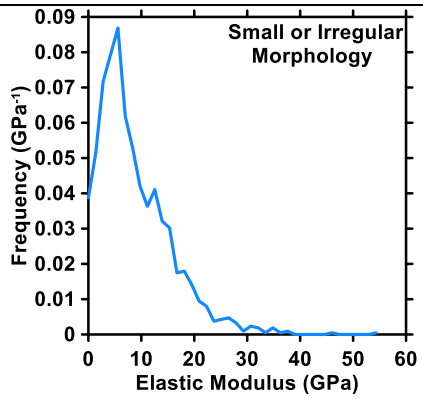

(d)

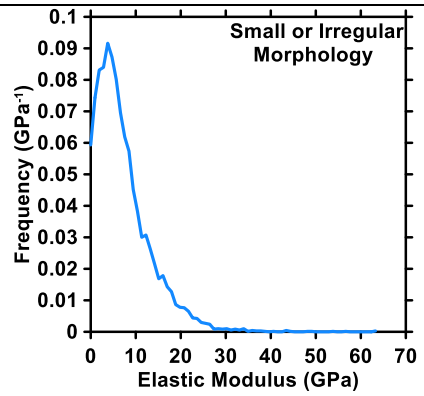

(e)

Figure 7. Another example of elastic modulus analysis of MSH sample as similar to what is already shown in the **Fig. 6**, showing **(a)** elastic modulus map, **(b)** cropped-in graph for faceted morphology of MSH at 64 GPa, **(c)** cropped-in graph for faceted morphology of MSH at 64 GPa, **(d)** cropped-in graph for irregular morphology of MSH at 6 GPa, **(e)** cropped-in graph for irregular morphology of MSH at 6 GPa.

synthesized using chemical vapor deposition, and their elastic modulus was measured at 76.6 ± 2 GPa through nanoscale three-point bending tests with an atomic force microscope. The nanowires exhibited brittle fracture failure in bending.[40] Additionally, the elastic properties of silica glass were determined via molecular dynamic simulation, resulting in an elastic modulus of 72.56 GPa based on the slope of the initial linear segment.[41]

The effect of reaction time on the development or formation of MSH precipitates on mica surfaces was studied and its subsequent influence on the elastic modulus was examined. To comprehend how different reaction times affected the formation of MSH precipitates (seen in **Fig. 8a and 8b**), several reaction times were investigated. For this analysis, similar supersaturated solutions of MSH with a final concentration of 100 mM were used to react with the mica surface. Two different reaction durations were considered: one with a reaction time of 40 minutes (**Fig. 8a**) and the other with a prolonged reaction time of 48 hours (**Fig. 8b**). The shorter reaction time resulted in the formation of precipitates with limited structural complexity. However, the sample that was kept for 48 hours of reaction time shows a combination of irregular or small and faceted or big morphological characteristics (**Fig. 8d**). This suggests that the extended reaction time allowed for the development or formation of precipitates with greater structural diversity. As we saw in the earlier observations made in **Figure. 6**, where it was established that irregular or small morphological characteristics correspond to lower elastic modulus values, and faceted or big morphological characteristics are associated with higher elastic modulus values. The result from this analysis determined that the sample with a reaction time of 40 minutes exhibited a relatively low elastic modulus value, approximately 10 GPa (**Fig. 8e**). This result is in line with the presence of predominantly irregular or small morphological characteristics. Whereas the sample subjected to a longer reaction time of 48 hours showed a significantly higher elastic modulus value, approximately 57.2 GPa (**Fig. 8f**).

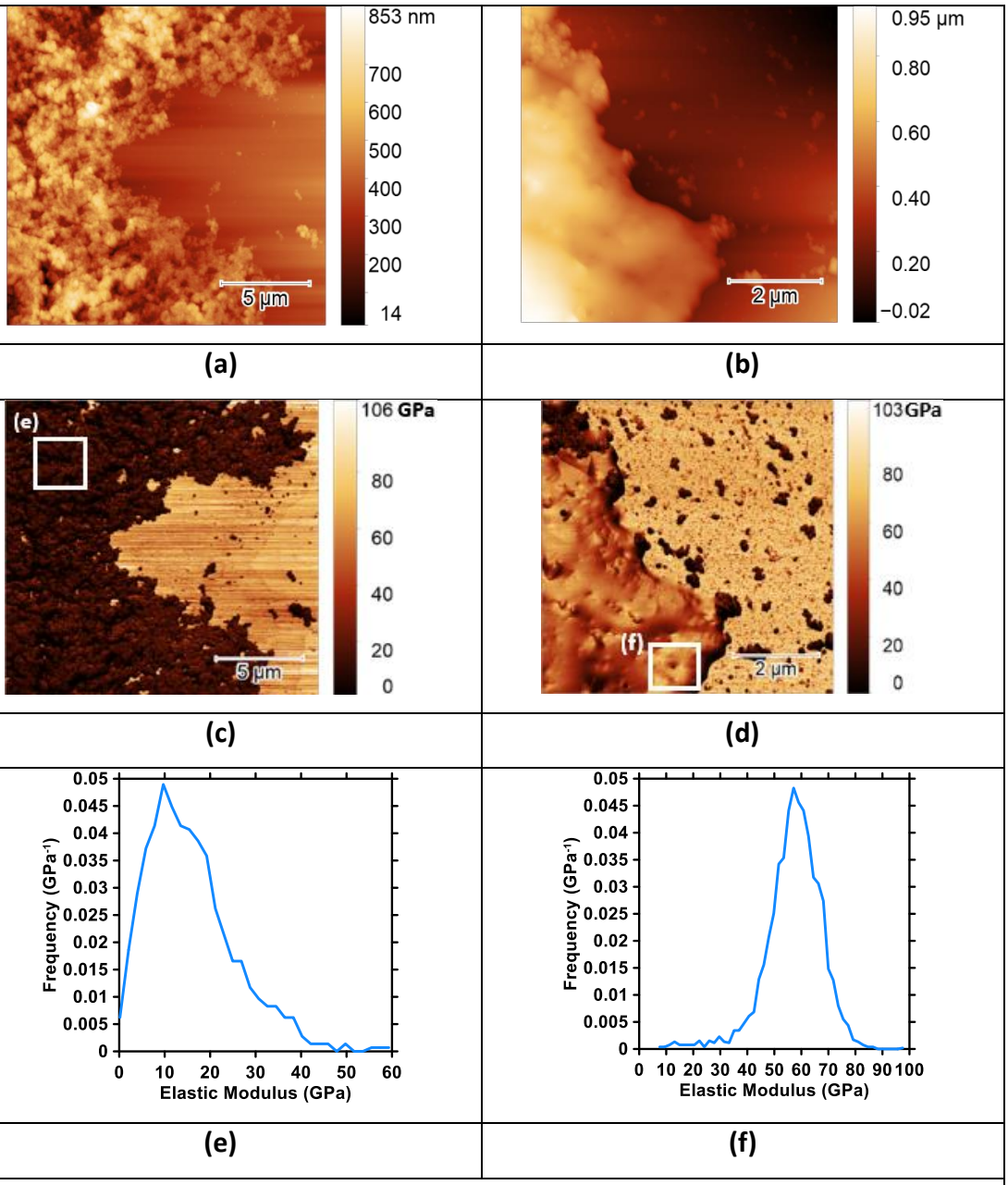

Figure 8. AFM images of MSH precipitates grown on mica substrate after reacting for 40 mins & 48 hours at 25 °C with final concentration of Mg = 100 mM; Si = 100 mM; Mg/Si = 1, taken using AM-FM mode, showing **(a)** height map for 40 mins reaction time, **(b)** height map for 48 hours reaction time, **(c)** elastic modulus map for 40 mins reaction time, **(d)** elastic modulus map for 48 hours reaction time, **(e)** elastic modulus graph for 40 mins reaction time showing MSH as 10 GPa, and **(f)** elastic modulus graph for 48 hours reaction time showing grown MSH with EM as 57.2 GPa.

3.3. *Understanding Elastic modulus variation as a function of Mg/Si molar ratios.*

Experimental investigations were conducted on multiple MSH samples, each characterized by one of four distinct Mg/Si molar ratios: 0.5, 1, 1.5, and 2 (**Fig. 9**). Furthermore, a mathematical fit was applied to the data points to provide a more detailed representation of the relationship. For MSH samples exhibiting faceted or big morphological characteristics, as the Mg/Si molar ratios increased across the range from 0.5 to 2, the elastic modulus values decrease a little but are near constant, seemingly unaffected by the variations in Mg/Si molar ratios with a range of 40-64 GPa (**Fig. 9**). However, MSH samples characterized by irregular or small morphological features exhibited a different pattern. With increasing Mg/Si molar ratios, the elastic modulus values for these samples exhibited a slight decrease with a range of 5-15 GPa (**Fig. 9**). This observation indicates that the morphological characteristics of MSH are intimately tied to its mechanical properties and response to changes in Mg/Si molar ratios.

To better understand why elastic modulus of MSH varies as a function of Mg/Si molar ratios, especially decreasing as the Mg/Si ratio increases, let us consider a CSH (calcium silicate hydrate) system: a different system that is exactly like MSH. The previous studies on synthesis of CSH, it is proven that, as the Ca/Si ratios increases, the length of the silicate chains decreases,[42,43] considering the models that describe the structure of CSH, particularly the nature of nano-crystallites and intra-lamellar interactions. It is also proven that synthesized CSH have the effect of Ca/Si ratios on the Q2/Q1(types of connections between SiO_4 tetrahedra) ratio, and consequently on the mean length of silicate chains of CSH, observing as the ratios are decreased there was an increase in length of silicate chains, principally for a Ca/Si ratio less than 1. Therefore, it is likely that the mechanical properties (elastic modulus) vary according to the Ca/Si ratio.[44] Another study was conducted using forcefield atomistic techniques to model the CSH structure, it was observed that the elastic modulus of CSH increases with an increasing average length of silicate chains, when the Ca/Si molar ratio decreases.[45]

FT-IR analysis from the previous study confirmed the theory that a reduction in the Ca/Si ratio increases the degree of polymerization of silica tetrahedra,[44,45] where the presence of type Q1 and Q2 connections occurred for lower Ca/Si ratio of 0.7 and a reduction in the spectrum in Q2 for higher Ca/Si ratio of 2.1 was observed, indicating a lower degree of polymerization.[46] This

clearly means that higher the degree of polymerization, higher the elastic modulus values, and vice versa. Even though it is known that increasing the Ca/Si ratio promotes axial growth, decreases the interplanar distance, and increases density, all of which increase CSH strength, experimental results show that one of the most crucial elements influencing material strength is the composition of the particle packing. CSH's mechanical characteristics are impacted by changes in the Ca/Si ratio. CSH's micro- and nano-porosity may have an impact on this behavior. On the other hand, the Ca/Si ratio may have affected the particle packing shape and characteristics.[46]

Upon a comprehensive examination of the factors interpreted for the decrease in elastic modulus with increasing Ca/Si ratios, a similar pattern is observed in MSH (magnesium silicate hydrate) samples. The observed reduction in elastic modulus values in MSH samples correlates with elevated Mg/Si ratios, analogous to the trend in C-S-H. This insight carries profound implications in scientific and engineering domains, showcasing the potential for precise manipulation of the mechanical properties of MSH-based materials. This manipulation, particularly in construction and geotechnical applications, becomes feasible through the deliberate control of both morphological characteristics and the Mg/Si molar ratios, offering avenues for tailoring material performance to specific requirements.

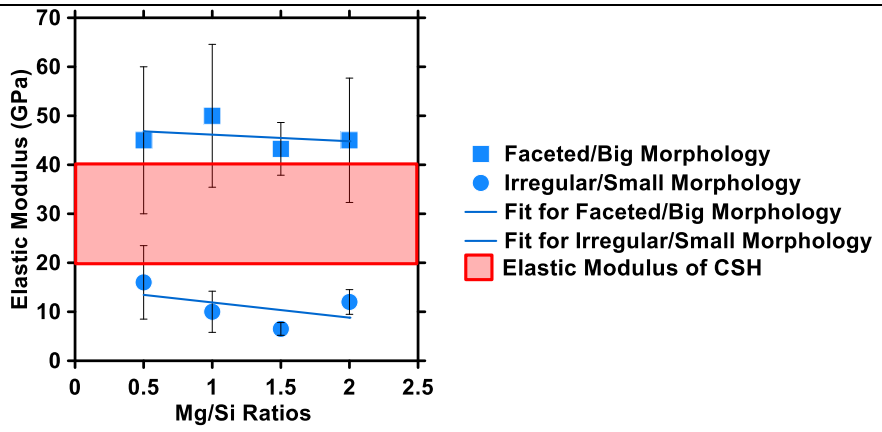

Figure 9. Influence of elastic modulus of MSH under different Mg/Si ratios, and comparison of elastic modulus of MSH with CSH

3.4. Comparison of MSH results with CSH data.

The elastic modulus values for MSH, when considering two distinct morphological characteristics, namely irregular or small and faceted or big, exhibit specific ranges. For MSH with irregular or small morphological characteristics, the elastic modulus typically falls within the range of 5-15 GPa. However, MSH samples with faceted or big morphological characteristics demonstrate higher elastic modulus values, which typically range between 40-64 GPa, and in some areas, can approach an impressive 75 GPa, as discussed in **sections 3.2 and 3.3** and depicted in **Figure 9**. In the broader context of materials used in construction, a relevant point of comparison is the elastic modulus of CSH (Calcium Silicate Hydrate), which has been determined through prior research. Typically, CSH exhibits elastic modulus values that fall within the range of 20-40 GPa.[47]

The elevated elastic modulus exhibited by MSH (magnesium silicate hydrate) arises from its sheet-like molecular structure, such as phyllosilicates. This structural configuration, characterized by a layered arrangement, imparts higher stiffness and strength to MSH. This observation aligns with established principles in material science, where sheet-like structures contribute to enhanced mechanical properties. In contrast, CSH (calcium silicate hydrate) displays lower elastic modulus values due to its chain-like molecular structure, such as inosilicates. The chain-like arrangement in CSH results in a lower degree of polymerization, a critical factor influencing elastic modulus. Moreover, MSH is predominantly Q3 dominant, indicating a higher degree of polymerization. As discussed in **section 3.3**, a high degree of polymerization is associated with increased elastic modulus values.

This finding holds substantial significance for the field of construction materials. The higher elastic modulus of MSH implies that it possesses enhanced stiffness and rigidity when compared to CSH. This has profound implications for its potential utility as a cementitious material in various construction applications. A material with a higher elastic modulus can offer enhanced structural integrity, reduced deformation under load, and improved resistance to cracks or damage, all of which are highly desirable attributes in construction. As a result, MSH, with its impressive elastic modulus values, especially in cases of faceted or big morphological characteristics, emerges as a promising and highly relevant cementitious material for use in a

wide range of construction applications. Its mechanical properties can contribute to the development of more durable and resilient structures, aligning with the evolving needs and standards of the construction industry.

CONCLUSION

In conclusion, our comprehensive investigation into MSH (magnesium silicate hydrate) synthesis and characterization through techniques such as XRD (X-ray Diffraction), TGA (Thermogravimetric Analysis), FT-IR (Fourier-Transform Infrared), SEM-EDS (Scanning Electron Microscope - Energy Dispersive X-ray Spectroscopy), and AFM (Atomic Force Microscopy) provided detailed insights into its composition, structure, and evolution. XRD identified low crystalline phases, consistently present across various Mg/Si ratios, with distinctive broad humps for MSH and tiny intense peaks for brucite, suggesting the presence of brucite in very small quantity that too as an initial reaction product and later contributing to the formation of MSH. TGA revealed the thermal behavior of MSH, highlighting weight loss linked to water content, silanol, and magnesium hydroxyl groups, emphasizing its nano-crystalline structure. FT-IR confirmed the presence of brucite in small quantities, particularly in lower Mg/Si ratios, while SEM-EDS displayed a homogeneous distribution of Mg and Si. AFM analysis identified two distinct morphological features in MSH samples (Mg/Si ratio of 1): irregular or small and faceted or large morphology, each associated with distinct elastic modulus values ranging from 5-15 GPa and 40-64 GPa, respectively. These modulus values exhibited an increasing trend with longer reaction times, lower Mg/Si ratios, and higher degree of polymerization, highlighting the influence on mechanical properties (elastic modulus). Remarkably, MSH demonstrated superior elastic modulus values because of its sheet-like molecular structure, leading to higher degree of polymerization compared to chain-like molecular structure, leading to lower degree of polymerization for CSH (calcium silicate hydrate), a common component in cementitious materials, suggesting its promising potential for diverse applications in the construction industry.

REFERENCES

(1) E. Gartner, M. Gimenez, V. Meyer, A. Pisch, A Novel Atmospheric Pressure Approach to the Mineral Capture of CO2 from Industrial Point Sources, Thirteenth Annual Conference on Carbon Capture, Utilization and Storage, Pittsburgh, Pennsylvania, 2014.

(2) F. Zhang, Magnesium Oxide Based Binders as Low-Carbon Cements (PhD Thesis) Imperial College London, 2012.

(3) L. Vandeperre, M. Liska, A. Al-Tabbaa, Hydration and Mechanical Properties of Magnesia, Pulverized Fuel Ash, and Portland Cement Blends, J. Mater. Civ. Eng. 20 (2008) 375–383.

(4) Dylan Singh 1,2, Trinh Thao My Nguyen 1,3, Evann Bustamantes 1,2,4, Abdul Wahab 1,2,; Ahmad Hamzah Yousaf 1,2,4, Ian Shortt 1,2, Frank W. Foss, Jr.3, Maria Konsta–Gdoutos 2,5, Sang Soo Lee,6 Erika Callagon La Plante 1,2,*. Chemical Structure and Complex Growth Modes of Magnesium Silicate Hydrate: Nanoparticle Orientation, Aggregation, and Fusion.

(5) Mohamad, N.; Muthusamy, K.; Embong, R.; Kusbiantoro, A.; Hashim, M. H. Environmental Impact of Cement Production and Solutions: A Review. *Materials Today: Proceedings* **2022**, *48*, 741–746. https://doi.org/10.1016/j.matpr.2021.02.212.

(6) Tyrrell, T. Calcium Carbonate Cycling in Future Oceans and Its Influence on Future Climates. *Journal of Plankton Research* **2007**, *30* (2), 141–156. https://doi.org/10.1093/plankt/fbm105.

(7) Huntington, T. G. The Potential for Calcium Depletion in Forest Ecosystems of Southeastern United States: Review and Analysis. *Global Biogeochemical Cycles* **2000**, *14* (2), 623–638. https://doi.org/10.1029/1999GB001193.

(8) *Soil-Calcium Depletion Linked to Acid Rain and Forest Growth in the Eastern United States*; 1999. https://doi.org/10.3133/wri984267.

(9) Tan-Trac, Nguyen, and Huu-Tai, Thai, et al. “Optimised Mix Design and Elastic Modulus Prediction of Ultra-High Strength Concrete”. CONSTRUCTION AND BUILDING MATERIALS, Vol.302, 2021, Pp. 14-. Doi:10.1016/j.Conbuildmat.2021.124150.

(10) Kocab, D.; Kucharczykova, B.; Misak, P.; Zitt, P.; Kralikova, M. Development of the Elastic Modulus of Concrete under Different Curing Conditions. *Procedia Engineering* **2017**, *195*, 96–101. https://doi.org/10.1016/j.proeng.2017.04.529.

(11) Korolev, A. S.; Kopp, A.; Odnoburcev, D.; Loskov, V.; Shimanovsky, P.; Koroleva, Y.; Vatin, N. I. Compressive and Tensile Elastic Properties of Concrete: Empirical Factors in Span Reinforced Structures Design. *Materials* **2021**, *14* (24), 7578. https://doi.org/10.3390/ma14247578.

(12) Wei Jiang, Dongdong Yuan, Shuangjiao Zhang, Rui Bao, Jingjing Xiao, Wangjie Wu, Teng Wang, Experimental Analysis of Deformation-Adapted Binders and Their Mixture Performance, Construction and Building Materials, Volume 389, 2023, 131733, ISSN 0950-0618,.

(13) Li P, Zhang Y, Duan S, Huang R, Gu J. Variation Pattern of the Elastic Modulus of Concrete under Combined Humidity and Heat Conditions. Materials (Basel). 2023 Aug 3;16(15):5447. Doi: 10.3390/Ma16155447. PMID: 37570153; PMCID: PMC10419823.

(14) AM-FM Viscoelastic Mapping Mode © Oxford Instruments Asylum Research Inc.

(15) Escalante-García, J. I.; Sharp, J. H. The Microstructure and Mechanical Properties of Blended Cements Hydrated at Various Temperatures. *Cement and Concrete Research* **2001**, *31* (5), 695–702. https://doi.org/10.1016/S0008-8846(01)00471-9.

(16) Kjellsen, K. O.; Detwiler, R. J.; Gjørv, O. E. Pore Structure of Plain Cement Pastes Hydrated at Different Temperatures. *Cement and Concrete Research* **1990**, *20* (6), 927–933. https://doi.org/10.1016/0008-8846(90)90055-3.

(17) Ben Haha, M.; Le Saout, G.; Winnefeld, F.; Lothenbach, B. Influence of Activator Type on Hydration Kinetics, Hydrate Assemblage and Microstructural Development of Alkali Activated Blast-Furnace Slags. *Cement and Concrete Research* **2011**, *41* (3), 301–310. https://doi.org/10.1016/j.cemconres.2010.11.016.

(18) Bernard, E.; Lothenbach, B.; Chlique, C.; Wyrzykowski, M.; Dauzères, A.; Pochard, I.; Cau-Dit-Coumes, C. Characterization of Magnesium Silicate Hydrate (M-S-H). *Cement and Concrete Research* **2019**, *116*, 309–330. https://doi.org/10.1016/j.cemconres.2018.09.007.

(19) Nied, D.; Enemark-Rasmussen, K.; L'Hopital, E.; Skibsted, J.; Lothenbach, B. Properties of Magnesium Silicate Hydrates (M-S-H). *Cement and Concrete Research* **2016**, *79*, 323–332. https://doi.org/10.1016/j.cemconres.2015.10.003.

(20) D.R.M. Brew, F.P. Glasser, Synthesis and Characterisation of Magnesium Silicate Hydrate Gels, Cem. Concr. Res. 35 (2005) 85–98.

(21) T. Zhang, L.J. Vandeperre, C.R. Cheeseman, Development of Magnesium Silicate Hydrate Cement System for Nuclear Waste Encapsulation, NUWCEM, Avignon 2011, Pp. 582–591.

(22) Simoni, M.; Woo, C. L.; Zhao, H.; Iuga, D.; Svora, P.; Hanein, T.; Kinoshita, H.; Walkley, B. Reaction Mechanisms, Kinetics, and Nanostructural Evolution of Magnesium Silicate Hydrate (M-S-H) Gels. *Cement and Concrete Research* **2023**, *174*, 107295. https://doi.org/10.1016/j.cemconres.2023.107295.

(23) Zhang, Y.; Li, Y.; Xu, Y.; Sang, S.; Jin, S. Enhanced Formation of Magnesium Silica Hydrates (M-S-H) Using Sodium Metasilicate and Caustic Magnesia in Magnesia Castables. *Ceramics International* **2017**, *43* (12), 9110–9116. https://doi.org/10.1016/j.ceramint.2017.04.058.

(24) Z. Li, T. Zhang, J. Hu, Y. Tang, Y. Niu, J. Wei, Q. Yu, 2014, Characterization of Reaction Products and Reaction Process of MgO–SiO2– H2O System at Room Temperature, Construction and Building Materials, 61, 252.

(25) D. Nied, K. Enemark-Rasmussen, E. L'Hopital, J. Skibsted, B. Lothenbach, Properties of Magnesium Silicate Hydrates (MSH), Cem. Concr. Res. 79 (2016) 323–332.

(26) C. Roosz, S. Grangeon, P. Blanc, V. Montouillout, B. Lothenbach, P. Henocq, E. Giffaut, P. Vieillard, S. Gaboreau, Crystal Structure of Magnesium Silicate Hydrates (MSH): The Relation with 2: 1 Mg–Si Phyllosilicates, Cem. Concr. Res. 73 (2015) 228–237.

(27) F. Jin, A. Al-Tabbaa, Thermogravimetric Study on the Hydration of Reactive Magnesia and Silica Mixture at Room Temperature, Thermochim. Acta 566 (2013) 162–168.

(28) A. Dumas, F. Martin, C. Le Roux, P. Micoud, S. Petit, E. Ferrage, J. Brendlé, O. Grauby, M. Greenhill-Hooper, Phyllosilicates Synthesis. Example of Synthetic Talc, Phys. Chem. Miner. 40 (2013) 361–373.

(29) R.L. Frost, J.T. Kloprogge, Infrared Emission Spectroscopic Study of Brucite, Spectrochim. Acta A Mol. Biomol. Spectrosc. 55 (1999) 2195–2205.

(30) B. Lothenbach, D. Nied, E. L'Hôpital, G. Achiedo, A. Dauzères, Magnesium and Calcium Silicate Hydrates, Cem. Concr. Res. 77 (2015) 60–68. Https://Doi.Org/10.1016/j.Cemconres.2015.06.007.

(31) M.R. Marsiske, C. Debus, F. Di Lorenzo, E. Bernard, S.V. Churakov, C. Ruiz-Agudo, Immobilization of (Aqueous) Cations in Low pH M-S-H Cement, Appl. Sci. 11 (2021) 2968. Https://Doi.Org/10.3390/App11072968.

(32) E. Bernard, B. Lothenbach, D. Rentsch, I. Pochard, A. Dauzères, Formation of Magnesium Silicate Hydrates (M-S-H), Phys. Chem. Earth Parts ABC. 99 (2017) 142–157. Https://Doi.Org/10.1016/j.Pce.2017.02.005.

(33) F.A. Miller, C.H. Wilkins, 1952, Infrared Spectra and Characteristic Frequencies of Inorganic Ions, Analytical Chemistry, 24, 1253- 1294.

(34) Brew, D. R. M.; Glasser, F. P. Synthesis and Characterisation of Magnesium Silicate Hydrate Gels. *Cement and Concrete Research* **2005**, *35* (1), 85–98. https://doi.org/10.1016/j.cemconres.2004.06.022.

(35) N. Dominik, E.R. Kasper, L. Emilie, Properties of Magnesium Silicate Hydrates (M-S-H), Cem. Concr. Res. 79 (2016) 323–332.

(36) T. Zhang, L.J. Vandeperre, C.R. Cheeseman, Formation of Magnesium Silicate Hydrate (M-S-H) Cement Pastes Using Sodium Hexametaphosphate, Cem. Concr. Res. 65 (2014) 8–14.

(37) Catti, M.; Ferraris, G.; Hull, S.; Pavese, A. Static Compression and H Disorder in Brucite, Mg(OH)2, to 11 GPa: A Powder Neutron Diffraction Study. *Phys Chem Minerals* **1995**, *22* (3). https://doi.org/10.1007/BF00202300.

(38) Jiang, F.; Speziale, S.; Duffy, T. S. Single-Crystal Elasticity of Brucite, Mg(OH)2, to 15 GPa by Brillouin Scattering. *American Mineralogist* **2006**, *91* (11–12), 1893–1900. https://doi.org/10.2138/am.2006.2215.

(39) Juhyuk Moon, Sergio Speziale, Cagla Meral, Bora Kalkan, Simon M. Clark, Paulo J.M. Monteiro, Determination of the Elastic Properties of Amorphous Materials: Case Study of Alkali–Silica Reaction Gel, Cement and Concrete Research, Volume 54, 2013, Pages 55-60, ISSN 0008-8846,.

(40) Ni, H.; Li, X.; Gao, H. Elastic Modulus of Amorphous SiO2 Nanowires. *Applied Physics Letters* **2006**, *88* (4), 043108. https://doi.org/10.1063/1.2165275.

(41) Https://Www.Rsc.Org/Suppdata/Sm/C4/C4sm01074d/C4sm01074d1.Pdf.

(42) Richardson, I. G.Cem. Concr. Res.2008,38, 137−158.

(43) Pellenq, R. J. M.; Van Damme, H.MRS Bull.2004,5, 319−323.

(44) Beaudoin, J. J.; Raki, L.; Alizadeh, R. A.Cem. Concr. Compos.2009,31, 585−600.

(45) Manzano, H.; Dolado, J. S.; Ayuela, A.Acta Mater.2009,57,1666−1675.

(46) Pelisser, F.; Gleize, P. J. P.; Mikowski, A. Effect of the Ca/Si Molar Ratio on the Micro/Nanomechanical Properties of Synthetic C-S-H Measured by Nanoindentation. *J. Phys. Chem. C* **2012**, *116* (32), 17219–17227. https://doi.org/10.1021/jp302240c.

(47) Xu, J.; Corr, D. J.; Shah, S. P. Nanomechanical Properties of C-S-H Gel/Cement Grain Interface by Using Nanoindentation and Modulus Mapping. *Journal of Zhejiang University-SCIENCE A* **2015**, *16* (1), 38–46. https://doi.org/10.1631/jzus.A1400166.